Terahertz photoconductive antenna with metal nanoislands

Sang-Gil Park,[1,2,3] Yongje Choi,[1,3] Young-Jae Oh,[1] and Ki-Hun Jeong[1,2,*]

[1]*Department of Bio and Brain Engineering, Korea Advanced Institute of Science and Technology (KAIST), 291 Daehak-ro, Yuseong-gu, Daejeon 305-701, South Korea*

[2]*KAIST Institute for Optical Science and Technology, Korea Advanced Institute of Science and Technology (KAIST), 291 Daehak-ro, Yuseong-gu, Daejeon 305-701, South Korea*

[3]*These authors contributed equally to this work*

[*]*kjeong@kaist.ac.kr*

Abstract: This work presents a nanoplasmonic photoconductive antenna (PCA) with metal nanoislands for enhancing terahertz (THz) pulse emission. The whole photoconductive area was fully covered with metal nanoislands by using thermal dewetting of thin metal film at relatively low temperature. The metal nanoislands serve as plasmonic nanoantennas to locally enhance the electric field of an ultrashort pulsed pump beam for higher photocarrier generation. The plasmon resonance of metal nanoislands was achieved at an excitation laser wavelength by changing the initial thickness of metal film. This nanoplasmonic PCA shows two times higher enhancement for THz pulse emission power than a conventional PCA. This work opens up a new opportunity for plasmon enhanced large-aperture THz photoconductive antennas.

OCIS codes: (310.6628) Subwavelength structures, nanostructures; (110.6795) Terahertz imaging; (040.5150) Photoconductivity; (250.5403) Plasmonics.

References and links

1. M. Tonouchi, "Cutting-edge terahertz technology," Nat. Photonics **1**(2), 97–105 (2007).
2. E. Pickwell and V. P. Wallace, "Biomedical applications of terahertz technology," J. Phys. D Appl. Phys. **39**(17), R301–R310 (2006).
3. K. Kawase, Y. Ogawa, Y. Watanabe, and H. Inoue, "Non-destructive terahertz imaging of illicit drugs using spectral fingerprints," Opt. Express **11**(20), 2549–2554 (2003).
4. N. Nagai, R. Kumazawa, and R. Fukasawa, "Direct evidence of inter-molecular vibrations by THz spectroscopy," Chem. Phys. Lett. **413**(4-6), 495–500 (2005).
5. M. Exter, C. Fattinger, and D. Grischkowsky, "Terahertz time-domain spectroscopy of water vapor," Opt. Lett. **14**(20), 1128–1130 (1989).
6. R. M. Woodward, B. E. Cole, V. P. Wallace, R. J. Pye, D. D. Arnone, E. H. Linfield, and M. Pepper, "Terahertz pulse imaging in reflection geometry of human skin cancer and skin tissue," Phys. Med. Biol. **47**(21), 3853–3863 (2002).
7. M. Tani, S. Matsuura, K. Sakai, and S. Nakashima, "Emission characteristics of photoconductive antennas based on low-temperature-grown GaAs and semi-insulating GaAs," Appl. Opt. **36**(30), 7853–7859 (1997).
8. Y. C. Shen, P. C. Upadhya, E. H. Linfield, H. E. Beere, and A. G. Davies, "Ultrabroadband terahertz radiation from low-temperature-grown GaAs photoconductive emitters," Appl. Phys. Lett. **83**(15), 3117–3119 (2003).
9. A. Dreyhaupt, S. Winnerl, T. Dekorsy, and M. Helm, "High-intensity terahertz radiation from a microstructured large-area photoconductor," Appl. Phys. Lett. **86**(12), 121114 (2005).
10. B. Pradarutti, R. Müller, W. Freese, G. Matthäus, S. Riehemann, G. Notni, S. Nolte, and A. Tünnermann, "Terahertz line detection by a microlens array coupled photoconductive antenna array," Opt. Express **16**(22), 18443–18450 (2008).
11. S.-G. Park, K. H. Jin, M. Yi, J. C. Ye, J. Ahn, and K.-H. Jeong, "Enhancement of terahertz pulse emission by optical nanoantenna," ACS Nano **6**(3), 2026–2031 (2012).
12. C. W. Berry and M. Jarrahi, "Plasmonically-enhanced localization of light into photoconductive antennas," Proc. Conf. Lasers and Electro-Optics, CFI2 (2010)
13. H. Tanoto, J. Teng, Q. Wu, M. Sun, Z. Chen, S. Maier, B. Wang, C. Chum, G. Si, A. Danner, and S. J. Chua, "Greatly enhanced continuous-wave terahertz emission by nano-electrodes in a photoconductive photomixer," Nat. Photonics **6**(2), 121–126 (2012).

#175240 - $15.00 USD Received 30 Aug 2012; revised 20 Oct 2012; accepted 20 Oct 2012; published 25 Oct 2012

14. A. Geissler, M. He, J.-M. Benoit, and P. Petit, "Effect of hydrogen pressure on the size of nickel nanoparticles formed during dewetting and reduction of thin nickel films," J. Phys. Chem. C **114**(1), 89–92 (2010).
15. Y.-J. Oh and K.-H. Jeong, "Glass nanopillar arrays with nanogap-rich silver nanoislands for highly intense surface enhanced Raman scattering," Adv. Mater. (Deerfield Beach Fla.) **24**(17), 2234–2237 (2012).
16. S. Yang, F. Xu, S. Ostendorp, G. Wilde, H. Zhao, and Y. Lei, "Template-confined dewetting process to surface nanopatterns: fabrication, structural tunability, and structure-related properties," Adv. Funct. Mater. **21**(13), 2446–2455 (2011).
17. K. W. Vogt and P. A. Kohl, "Gallium arsenide passivation through nitridation with hydrazine," J. Appl. Phys. **74**(10), 6448–6450 (1993).
18. P. R. West, S. Ishii, G. V. Naik, N. K. Emani, V. M. Shalaev, and A. Boltasseva, "Searching for better plasmonic materials," Laser Photon. Rev. **4**(6), 795–808 (2010).
19. K. R. Catchpole and A. Polman, "Plasmonic solar cells," Opt. Express **16**(26), 21793–21800 (2008).
20. F. Stietz, J. Bosbach, T. Wenzel, T. Vartanyan, A. Goldmann, and F. Trager, "Decay times of surface plasmon excitation in metal nanoparticles by persistent spectral hole burning," Phys. Rev. Lett. **84**(24), 5644–5647 (2000).

1. Introduction

Terahertz (THz) radiation of 0.1 to 10 THz falls in the frequency gap between the infrared and microwaves. THz emission spectra have received much attention with technological advance such as high-power THz generation, THz imaging, and THz time-domain spectroscopy (TDS) [1]. In particular, THz pulses have many advantages in investigating material fingerprints through THz TDS because they can provide rich spectral information of diverse biochemical molecules at intermolecular or vibrational energy band [2–4]. However, THz technology has some technical limitations in a water-rich environment such as *in-vivo* biomedical applications due to high absorption from water molecules [5]. THz TDS with a reflection type can serve as an alternative method [6]; however, it still requires a high power terahertz emission source.

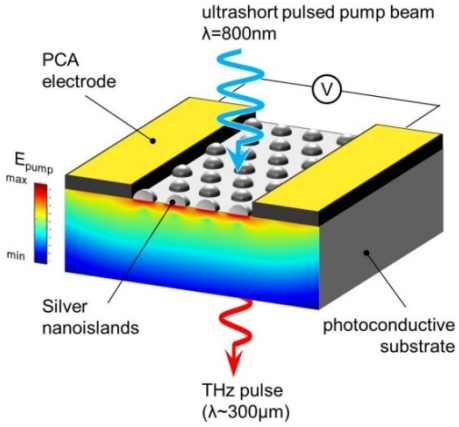

Fig. 1. A schematic diagram of nanoplasmonic photoconductive antenna (NP-PCA) with metal nanoislands. Plasmonic nanoislands are fabricated over the full photoconductive area to locally enhance the ultrashort pulsed pump beam. This local field enhancement increases photocarrier generation and THz pulse emission from the PCA.

Photoconductive antennas (PCAs) with an ultrashort pulse laser excitation are widely used as THz emission sources. THz pulse emission can be enhanced by incorporating either photoconductive materials with high acceleration of photo-excited carriers such as low-temperature grown gallium arsenide (LT-GaAs) [7,8] or by implementing constructive large-area excitation with inter-digital antennas and microlens arrays [9,10]. Recently, nanophotonics enables the enhancement of THz pulse emission by employing plasmonic nanoantennas between PCA electrodes [11–13]. The plasmonic nanostructures enhance the electric field of an ultrashort pulsed pump beam at localized surface plasmon resonance (LSPR). This local field enhancement increases photocarrier generation and THz pulse

#175240 - $15.00 USD Received 30 Aug 2012; revised 20 Oct 2012; accepted 20 Oct 2012; published 25 Oct 2012

emission from the PCA. However, the photoconductive area with plasmonic nanostructures is restricted due to high cost nanofabrication of metal nanostructures such as e-beam lithography. A cost-effective method is still required for THz photoconductive antennas with plasmon enhanced large-aperture.

This work presents a nanoplasmonic photoconductive antenna (NP-PCA) with metal nanoislands. Figure 1 illustrates a schematic diagram of NP-PCA with large-area excitation. When an ultrashort pulsed pump beam (λ = 800 nm) with photon energy higher than the band gap energy is injected onto a photoconductive substrate, the photocarriers are excited by the pump beam. The photocarriers generate a transient photocurrent as accelerated by the bias electric field between two PCA electrodes. This transient photocurrent induces THz pulse emission. Metal nanoislands over the whole photoconductive area serve as plasmonic nanoantennas for localizing the pump beam. This large-area local field enhancement of the pump beam finally results in the enhancement of THz pulse emission.

2. Nano and microfabrication of NP-PCA

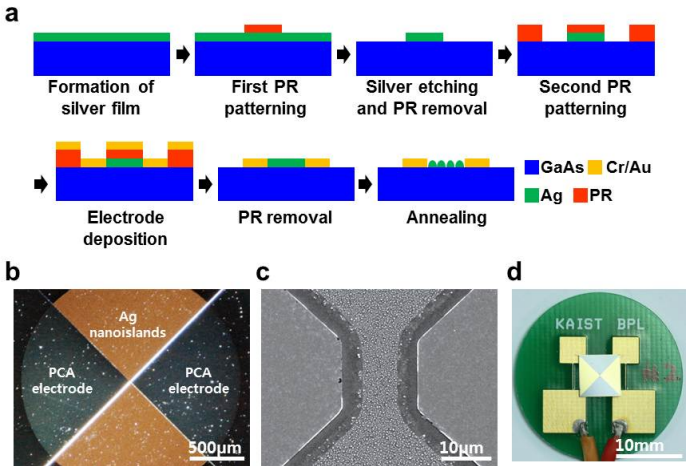

Fig. 2. (a) Hierarchical fabrication procedure for NP-PCA with Ag nanoislands. (b) A dark-field image of NP-PCA. The Ag nanoislands are highly scattered in red over the full photoconductive area due to LSPR at an excitation wavelength. (c) A SEM image of NP-PCA (photoconductive gap: 15 um in width). (d) NP-PCA packaged on a 1-inch printed circuit broad.

NP-PCA was fabricated by using thermal dewetting of thin metal film and metal lift-off to define the hierarchical structures over the whole photoconductive area at wafer level. Thermal dewetting of thin metal film was performed at relatively low temperature. This process has been recently utilized for the cost-effective and large-area fabrication of metal nanostructures in other applications such as carbon nanotube synthesis, nanogap fabrication, and surface-enhanced Raman spectroscopy [14–16]. A plasmonic material for thermal dewetting of thin film was selected by considering a photoconductive material and plasmon resonance. A semi-insulating gallium arsenide (SI-GaAs) wafer was used as a photoconductive substrate. SI-GaAs has many advantages for the PCA fabrication such as its short carrier lifetime, high carrier mobility, and high dark resistivity. However, metal dewetting at high temperature may cause thermal damages of GaAs such as a localized loss of volatile arsenic [17]. Therefore, Ag was used for dewetting of thin film to facilitate an easy formation of metal nanoislands within an upper limit of the annealing temperature. Compared to other metals, Ag also has a high quality factor of local field enhancement in visible wavelengths, which enables high local field enhancement with less absorption by metal nanoislands [18].

Figure 2(a) illustrates the hierarchical fabrication procedure of NP-PCA. First, thin Ag film was deposited on a 4 inch SI-GaAs substrate by using e-beam evaporation. The Ag film

#175240 - $15.00 USD Received 30 Aug 2012; revised 20 Oct 2012; accepted 20 Oct 2012; published 25 Oct 2012

was defined with a circular pattern on the full photoconductive area by using photolithography and chemical etching (TFS, Transcene). The PCA electrodes (Cr/Au) were then defined by using a conventional lift-off process. A bow-tie antennas with a 90° apex angle was selected for the NP-PCA due to relatively high power emission compared to other antennas. The Ag film was laterally etched to prevent electrical short-circuit between the PCA electrodes and the Ag nanoislands before the lift-off process. Finally, the Ag nanoislands were fabricated by thermal dewetting of thin Ag film. Figure 2(b) shows the dark-field image of NP-PCA. The Ag nanoislands on the top and bottom area are highly scattered in red due to LSPR. Figure 2(c) shows the SEM image of Ag nanoislands between the photoconductive electrodes. Ag nanoislands adjacent to the PCA electrodes were laterally removed by chemical etching. Here, the photoconductive gap is 15 μm and the width of photoconductive area with Ag nanoislands is 10 μm. The NP-PCA was mounted on a 1-inch printed circuit board for THz pulse emission measurement as shown in Fig. 2(d).

3. Plasmon resonance of silver nanoislands

THz pulse emission can be highly enhanced when the plasmon resonance of Ag nanoislands occurs at an excitation wavelength of 800 nm [11]. In this work, the plasmon resonance of Ag nanoislands was altered by the physical dimensions of metal nanostructures. The shape and size of Ag nanoislands were controlled by changing the initial thickness and the annealing temperature of thin Ag film for a constant time of 20 min. Figure 3 shows the SEM images of Ag nanoislands annealed at 350 °C with different initial thicknesses. The size of nanoislands increases with the initial thickness. For 20 nm thick Ag film, the average diameter of Ag nanoislands is ~173 nm. However, a 50 nm thick Ag film fails to be transformed into nanoislands during thermal dewetting. This failure results in an electric short circuit of the photoconductive area with high leakage current.

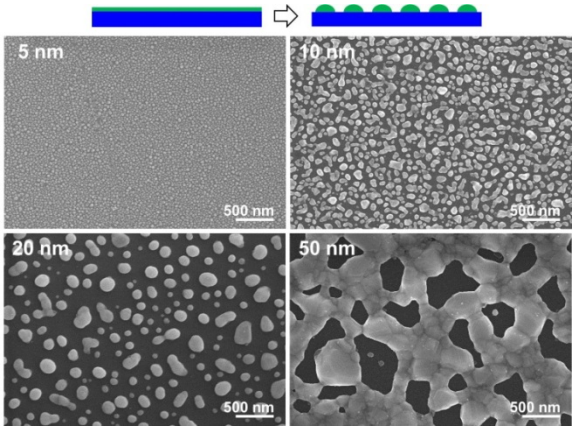

Fig. 3. SEM images of the Ag nanoislands transformed from different initial thicknesses of Ag films. The Ag films with an initial thickness below 20 nm were fully dewetted into nanoislands without an electric short circuit between PCA electrodes and the nanoislands size increases with the initial thickness.

The plasmon resonance of Ag nanoislands was investigated with dark-field micro-spectroscopy. The experimental set-up consists of a 50x dark-field lens (~NA 0.8), a dark-field adapter cube, and a spectrometer equipped with a charge-coupled device (CCD) camera as shown in Fig. 4(a). Figures 4(b) and 4(c) show the plasmonic scattering spectra of Ag nanoislands in visible range and the scattering intensity at an excitation wavelength of 800 nm, depending on the initial thickness and the annealing temperature. The results clearly demonstrate the LSPR peak of Ag nanoislands was red-shifted from 560 nm to 605 nm and broadened to the excitation wavelength as the initial thickness increases as shown in Fig. 4(b).

#175240 - $15.00 USD Received 30 Aug 2012; revised 20 Oct 2012; accepted 20 Oct 2012; published 25 Oct 2012

As the size of Ag nanoislands increases, conductive electrons move across the nanoislands in out-of-phase, so called dynamic depolarization. The dynamic depolarization reduces a restoring force of the conductive electrons and leads to the red-shift and broadening of LSPR peaks [19]. In addition, the enlarged size of Ag nanoislands results in a high scattering cross-section. Finally, the scattering intensity at the excitation wavelength increases with the initial thickness of Ag film as shown in Fig. 4(c). However, the maximum scattering value is achieved at the initial thickness of 20 nm because a 50 nm thick Ag film results in an electric short circuit. In this experiment, a 20 nm thick Ag film was used for the fabrication of NP-PCA.

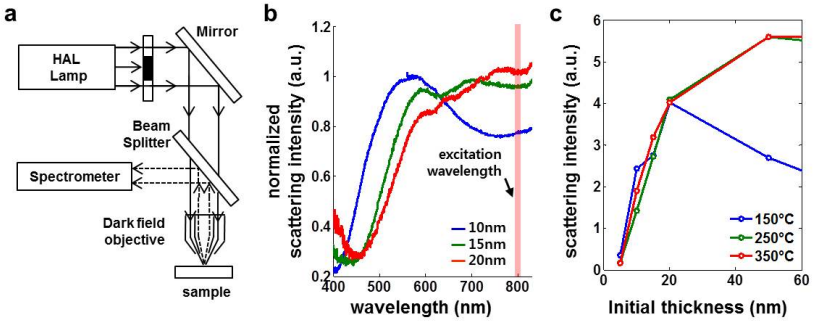

Fig. 4. Experimental setup for dark-field spectroscopy and plasmonic properties of Ag nanoislands. (a) The experimental setup. (b) Normalized scattering spectra of Ag nanoislands depending on the initial thickness of Ag film. (c) Plasmonic scattering intensity of Ag nanoislands at an excitation wavelength of 800 nm depending on initial thickness and the annealing temperature.

4. Measurement of THz pulse emission

THz pulses emitted from the NP-PCA were measured with a conventional electro-optic sampling method. A mode-locked Ti:Sapphire femtosecond laser generates 10 fs pulses with 100 MHz of repetition rate. The center wavelength is 800 nm, and the average power is 150 mW. The ultrashort pulses are split to a pump pulse beam and a probe pulse beam. The pump pulse beam was normally incident on the photoconductive area of NP-PCA. The NP-PCA was biased with square-wave voltage (f = 68 kHz, V_{pp} = 11 V) for a phase modulation measurement. The emitted THz pulses were collected by two parabolic mirrors and focused on a (110) ZnTe crystal of 1 mm in thickness. A probe pulse impinged onto the ZnTe crystal with the THz pulses. The polarization of the probe beam was modulated by the amplitude of THz pulses passing through the ZnTe crystal. This polarization change was detected by two photodetectors with a lock-in-amplifier. A silicon lens was not mounted on the backside of the PCAs to eliminate the misalignment artifact. The measured THz time-domain waveforms were 4 times averaged for high signal-to-noise ratio.

Figure 5 shows the time-domain waveforms and the power spectra of THz pulses emitted from the NP-PCA and a conventional PCA (C-PCA). The C-PCA was also prepared on a SI-GaAs substrate with the same configuration of NP-PCA except for Ag nanoislands. The power spectra were calculated by Fourier transformation of THz time-domain waveforms. The THz time-domain waveforms show a rapid increase of the peak amplitude due to the Ag nanoislands. This result explains that photocarrier transition rate is enhanced by LSPR of Ag nanoislands. The peak-to-peak amplitude of the THz time-domain waveform was enhanced by 1.4 times compared to that of C-PCA. The overall shape of THz time-domain waveforms was maintained. In other words, the enhancement of THz spectral power was observed along the whole spectral bandwidth of 0.1 – 1.1 THz and the average enhancement factor is ~2 times. The bandwidth reduction of THz spectra was not observed in this experiment. The interaction time between the incident photons and the electrons can be increased in a

#175240 - $15.00 USD Received 30 Aug 2012; revised 20 Oct 2012; accepted 20 Oct 2012; published 25 Oct 2012

photoconductive substrate by the surface plasmon of Ag nanoislands. However, the lifetime of Ag nanoislands are sufficiently short (~10 fs) not to affect the bandwidth compared to the THz pulse width (~1 ps) [11,20]. Based on a simple model for THz emission from a PCA, called "current surge model", the THz field amplitude is given as E~d/dt(*env*), where *n* is the carrier density and *v* is draft velocity. The carrier density can be then calculated from the energy density absorbed in a photoconductive substrate, $\mathrm{Im}(\varepsilon)|E|^2/2$. Whereas Ag nanoislands locally concentrate light between Ag nanoislands and the enhanced local field contributes to the enhancement of the photocurrent, the light concentration reduces the local electric field beneath the Ag nanoislands and finally results in low carrier density. However, the low carrier density beneath Ag nanoislands does not affect the total photocurrent because Ag nanoislands serve as a perfect conductor in the bias electric field. The detail of analytical description is also explained in our previous work [11]. In addition, Ag nanoislands may also decrease the breakdown voltage between PCA electrodes because Ag nanoislands increase the bias electric field among Ag nanoislands and PCA electrodes. However, the measured breakdown voltage of NP-PCA with Ag nanoislands is larger than 120 V.

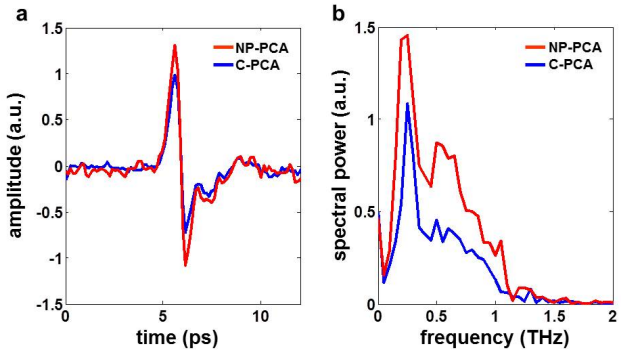

Fig. 5. (a) Time-domain waveforms of THz pulses emitted from NP-PCA with nanoislands and a conventional PCA (C-PCA) without Ag nanoislands over a photoconductive area. (b) THz power spectra from NP-PCA and C-PCA. The average emission power is enhanced by 2 times over 0.1-1.1 THz bandwidth.

5. Conclusion

In summary, this work demonstrates plasmon-enhanced terahertz pulse emission by photoconductive antenna with Ag nanoislands. Ag nanoislands were hierarchically fabricated at wafer-level by using thermal dewetting of thin Ag film. The plasmon resonance of Ag nanoislands was achieved at an excitation laser wavelength by changing the initial thickness of Ag film. An ultrashort pulsed pump beam is locally enhanced by Ag nanoislands at localized surface plasmon resonance. As a result, the PCA with plasmonic nanoislands shows two times higher THz pulse emission power compared to a conventional PCA. This cost-effective method is not limited for a single photoconductive antenna, but it can be also applied for large-aperture photoconductive antennas with constructive interference to provide a full opportunity for high-power THz pulse emission.

Acknowledgments

This work was supported by the National Research Foundation of Korea (NRF) grant funded by Korea government (MEST) (2011-0031868, 2012-0005641, 2012-0006653).

#175240 - $15.00 USD Received 30 Aug 2012; revised 20 Oct 2012; accepted 20 Oct 2012; published 25 Oct 2012